Journal of Electroceramics 1:1, 15–26, 1997

A Model to Predict Ionic Disorder and Phase Diagrams: Application to CaO-MgO, Gd_2O_3-ZrO_2, and to Sodium β''-alumina

G. CEDER, P.D. TEPESCH, A.F. KOHAN & A. VAN DER VEN
Department of Materials Science and Engineering, Massachusetts Institute of Technology, 77 Massachusetts Ave, Cambridge MA 02139

Received August 7, 1996; Revised November 8, 1996; Accepted November 14, 1996

Abstract. A model for the computation of ionic disorder and phase diagrams in complex oxides is presented. The model is based on a successive integration of the degrees of freedom in the material and can be combined with first-principles techniques to make predictions without the need for experimental data. We show applications on CaO-MgO, Gd_2O_3-ZrO_2, and sodium β''-alumina. For CaO-MgO the solid solubility limits are predicted in good agreement with experiments. both Gd_2O_3-ZrO_2 and sodium β''-alumina show a coupled order-disorder transition where two sublattices undergo an ordering transition simultaneously.

Keywords: phase diagram, first-principles, stabilized ZrO_2, diffusion, ordering, entropy

1. Introduction

The calculation of phase diagrams represents one of the most difficult challenges in ab-initio atomistic modeling. Whereas zero-temperature energies and structural properties can now be predicted with fair accuracy by means of first-principle calculations, non-zero temperature properties such as free energies, configurational disorder and phase transitions are far more difficult to obtain from first-principles. Molecular Dynamics presents one possibility for studying materials at non-zero temperature. The short duration of a typical Molecular Dynamics simulation (10–1000 ps) prevents the study of any property that is determined by the behavior of the material over long times. Finding equilibrium states and calculating free energies is therefore not within the reach of this technique. In addition, the computational expense of Molecular Dynamics with a first-principles Hamiltonian is very high, so that it is usually used with a more simple energy model.

In this paper we develop a model for the equilibrium thermodynamic and structural properties of a material that can be implemented with any energy function, including first-principle models. We show its application to the CaO-MgO system, Gd_2O_3-doped ZrO_2, and sodium β''-alumina systems. The idea behind the model is that although excitations on every time scale contribute to the non-zero temperature behavior, it is not necessary to know the detailed motions associated with every degree of freedom of the system. By separating the fast from the slow degrees of freedom, a model with only the slow degrees of freedom can be used to simulate the material over very long times. For the model to represent a specific material realistically, the Hamiltonian (the equation of motion) for the slow degrees of freedom must contain the effect of the faster degrees of freedom. As will be demonstrated below, this bridging of the time-scales for the thermodynamics of oxides can be achieved by coarse-graining the partition function.

2. Coarse-grained lattice models and the cluster expansion

At non-zero temperatures, macroscopic properties such as crystal structure, volume, order parameters, etc. are determined by the value that minimizes the *free energy*. Free energy is much more difficult to compute than *internal energy*, as the former contains

all the entropic contributions arising from disorder in the material. In a typical oxide mixture this disorder can be due to electronic excitations, vibrations, and substitutional excitations. An example of the latter is Frenkel disorder. In magnetic systems, disorder of the magnetic moments may also contribute to the entropy. Usually, the time scale for the various types of disorder is very different, with the substitutional one typically being the slowest. One can therefore picture a partially disordered oxide material as slowly moving from one substitutional configuration into another, while at each substitutional state quickly going through all the faster degrees of freedom. Our objective is to define a Hamiltonian that describes the substitutional degrees of freedom of the system, as this is the slowest time-scale. It is only possible to define a state function for the substitutional configurations, such as the Hamiltonian, if the fast and substitutional excitations are uncorrelated. This means that, in a given substitutional state, the system has no memory of how it arrived there. Given that the fast excitations such as vibrations are usually 4 to 5 orders of magnitude faster than substitutional excitations, this condition is usually easily fulfilled: in statistical mechanical terms, the system can be considered ergodic in its fast degrees of freedom, between slow excitations. This will make it possible to define an effective free energy contribution from the fast excitations in every substitutional state [1].

To obtain an effective Hamiltonian for the substitutional arrangement in a system, the partition function of the material can be coarse-grained to the partition function of a lattice model [1]. Let $\{\sigma\}$ indicate a given substitutional configuration and $\{fast\{\sigma\}\}$ a configuration of the faster degrees of freedom (vibrations, electronic excitations, etc.) that occur in that substitutional arrangement. The partition function (which defines the free energy) can be written as:

$$\begin{aligned} Z &= \sum_{all\ states} \exp\left(\frac{-E_{state}}{kT}\right) \\ &= \sum_{\sigma} \sum_{\{fast\{\sigma\}\}} \exp\left(\frac{-E(\{\sigma\},\{fast\{\sigma\}\})}{kT}\right) \end{aligned} \tag{1}$$

If all the fast degrees of freedom can be summed, this can be written as:

$$Z = \sum_{\{\sigma\}} \exp\left(\frac{-F(\{\sigma\})}{kT}\right) \tag{2}$$

with

$$F(\{\sigma\}) = -kT\ \ln\left[\sum_{\{fast\{\sigma\}\}} \exp\left(\frac{-E(\{\sigma\},\{fast\{\sigma\}\})}{kT}\right)\right] \tag{3}$$

$F(\{\sigma\})$ is the ''effective'' Hamiltonian for the substitutional degrees of freedom. As can be seen from Eq. (3) its value is given by the free energy resulting from all fast excitations in a given substitutional states. The most important entropic contributions to $F(\{\sigma\})$ come from vibrations and electronic excitations (for metallic systems). Equation (2) is the partition function of a lattice model and its corresponding free energy can therefore be calculated with standard lattice model techniques. If we use the correct definition for $F(\{\sigma\})$ this free energy is guaranteed to be the free energy of the real system. Equations (1)–(3) represent a successive reduction in the degrees of freedom by coarse-graining the partition function. In Eq. (2) only substitutional degrees of freedom remain with the faster degrees of freedom integrated into $F(\{\sigma\})$. The effective Hamiltonian $F(\{\sigma\})$ is an exponential average over all the energies of the fast excitations in the given substitutional state (Eq. (3)). Two problems remain: one needs an explicit form for $F(\{\sigma\})$, and it has to be possible to compute $F(\{\sigma\})$ for many configurations $\{\sigma\}$.

For real materials, there is no closed form for $F(\{\sigma\})$ and it is expanded in a basis of *cluster functions* [2]. If only two species can occupy a given lattice site i then a binary occupation variable σ_i can be defined for that site. The variable σ_i is $+1$ (-1) when site i is occupied by species A(B). Although the formalism can be extended to ternary occupations, we will exclude this generalization here for the sake of clarity [2–4]. The cluster functions are defined as:

$$\phi_\alpha = \prod_{i\in\alpha} \sigma_i \tag{4}$$

where α is any cluster of points on the lattice. The collection of ϕ_α can be shown to be orthogonal and to span all of configurational space so that it forms a suitable basis for functions that depend on the

substitutional configuration (such as $F(\{\sigma\})$). $F(\{\sigma\})$ can be expanded in this basis:

$$F(\{\sigma\}) = \sum_{\alpha} V_{\alpha}\phi_{\alpha}(\{\sigma\}) \tag{5}$$

The V_{α} are called effective cluster *interactions* (ECI). Since $F(\{\sigma\})$ is temperature dependent the V_{α} will also be temperature dependent.

The construction of a lattice Hamiltonian for a material now consists of finding the values for the V_{α} in the cluster expansion (Eq. (5)). The advantage of the cluster expansion lies in the fact that usually the ECI converge rapidly with the size of the cluster α and the separation of points in α. Many systems have been characterized by 10–15 ECI. Usually the ECI are determined by truncating the cluster expansion after some finite range and fitting the V_{α} to the computed values of $F(\{\sigma\})$ for a set of simple ordered configurations. In a typical procedure one will start the fit with a very small number of ECI and select additional ECI based on how much they improve the fit. This procedure is stopped when the fit does not improve much anymore. Of course, convergence always has to be checked by then comparing the value of $F(\{\sigma\})$ predicted by the cluster expansion with values from direct calculation for some configurations that were not used in the fit.

The cluster expansion can be extended to systems in which multiple sublattices contain substitutional disorder [5]. For example in Gd_2O_3-ZrO_2 , the Gd and Zr cations share a common sublattice while oxygen ions and charge compensating vacancies share the anion sublattice. In this case, an appropriate basis can be constructed from the cluster functions of each individual sublattice. If ϕ_{α} and θ_{β} are respectively the cluster function describing the binary disorder on the cation and anion sublattice, the new basis function:

$$\psi_{\alpha\beta} = \phi_{\alpha}\theta_{\beta} \tag{6}$$

can be defined for the complete system. This basis offers an unbiased description of the configuration of all ions and does not rely on any simplifying assumptions often used in modeling defects in oxides (such as models that assume association of isolated vacanies and dopant cations, etc.). We will use it to study coupled disorder in Gd_2O_3-ZrO_2 and in sodium β''-alumina.

$F(\{\sigma\})$ is itself defined from a partition function over the fast degrees of freedom. This partition function is made up out of a ground state and a series of excited states. Because including all the states in $F(\{\sigma\})$ can be difficult computationally, $F(\{\sigma\})$ is often approximated by the ground state energy. The ground state energy is the lowest energy that can be achieved for a given substitutional configuration of ions ($\{\sigma\}$). In almost all cases, this state can be obtained by starting with all ions at the sites of some underlying lattice and simply relaxing all coordinates and lattice parameters until a minimum for the energy is obtained. The single term approximation for $F(\{\sigma\})$ amounts to neglecting vibrational and electronic entropies. Although the former may represent a large contribution to the free energy, it is still under debate as to whether it is an important factor in the free energy *difference* between phases [6,7], which is the relevant quantity to study phase diagrams. Studies on model systems have indicated that neglecting the vibrations may lead to an overestimation of the temperature-scale by 10–25% [7].

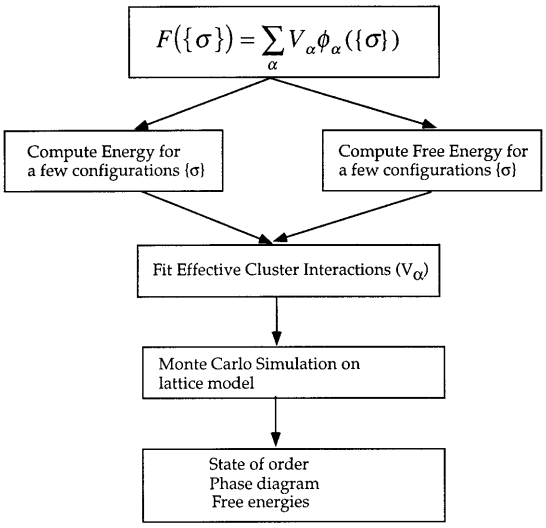

Fig. 1. Overview of the procedure to compute phase diagrams in systems with substitutional disorder.

An overview of the procedure to compute phase diagrams is given in Fig. 1. Note that a description for the energetics of the system is only needed to compute $E(\{\sigma\})$ or $F(\{\sigma\})$ for a number of configurations. Below we will demonstrate this procedure for three oxide systems.

3. CaO-MgO Solubility Limits

The experimentally determined phase diagram [8] of

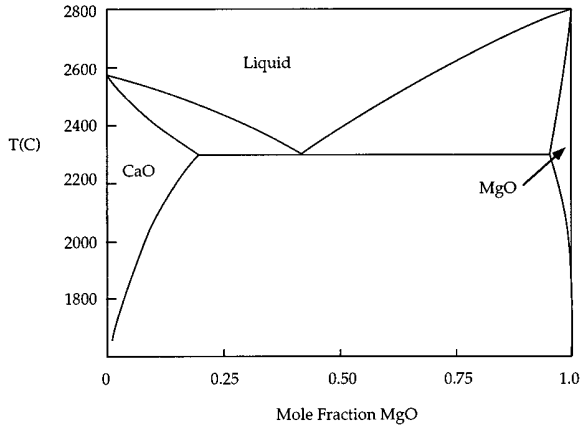

Fig. 2. Experimental phase diagram for the CaO-MgO system [redrawn from [8]].

the CaO-MgO system is shown in Fig. 2. We chose this system as it is well-characterized experimentally and relatively simple. It is therefore ideally suited as a system to benchmark our methods.

CaO and MgO both exist in the rocksalt structure. Mixing the compounds is therefore expected to lead to a substitutional arrangement of Ca and Mg ions on the cation sublattice. Because Ca and Mg have the same valence it can be safely assumed that the oxygen sublattice remains fully occupied. The substitutional degrees of freedom can therefore be modeled with an fcc lattice model representing the occupation of the cation sublattice [9].

A linear temperature dependence was chosen for the ECI. This is valid when the temperature is above its Debye temperature [10].

$$V_\alpha(T) = V_\alpha^{chem} + kTV_\alpha^{vib} \tag{7}$$

The chemical ECI (V_α^{chem}) are the expansion coefficients for the ground state energy as a function of configuration whereas the V_α^{vib} represent the contribution from lattice vibrations. Since CaO and MgO are wide band gap insulators there is no electronic contribution to $F(\{\sigma\})$.

To determine the chemical ECI in the cluster expansion we computed the energy of 21 ordered arrangements of the cations using a tight-binding Hamiltonian [11]. The tight binding Hamiltonian was derived from highly accurate pseudopotential calculations [12]. All symmetry-allowed degrees of freedom were fully relaxed. The 19 energy values were used to fit a cluster expansion with 14 ECI. To test convergence we also performed fits using only 18 of the 21 structures. The quality of the fit is judged by how well the fitted expansion then predicts the remaining three structures. In our case, the energy of all three structures was predicted to be within 4 meV of the correct value (calculated directly from the tight binding). More details can be found in [11]. The vibrational contribution to the ECI was determined from the phonon density of states of 3 ordered arrangements (in addition to pure CaO and MgO) [9]. The phonon spectra were computed using the Spherical Self-Consistent Atomic Deformation method (SSCAD) [13]. The solid state part of the CaO-MgO phase diagram was computed by performing a Monte Carlo simulation on the resulting lattice Hamiltonian. The result with and without the effect of vibrations is shown in Fig. 3. As we did not include the liquid, the solubility lines in CaO and MgO join to form a miscibility gap. The experimentally determined solubility limits are indicated with filled circles. Given that our theory is *ab-initio* and contains no adjustable parameters, the result is remarkably good. Without the vibrations the consolute temperature is 15–20% too high. Much of this is corrected by including the vibrational corrections. Even with a relatively small error in the temperature scale, the errors in the solubility limits are still relatively high since they depend exponentially on the energetics.

This benchmark study does however indicate that by combining an accurate energy model with lattice model statistical mechanics, very useful predictions

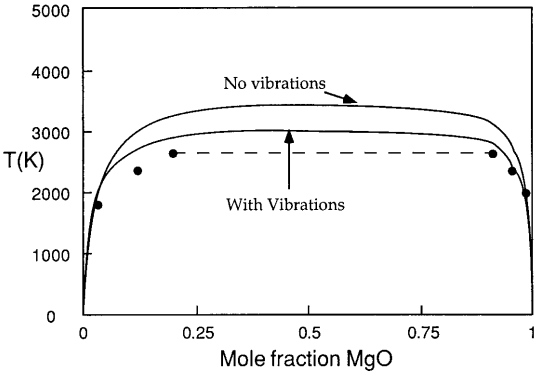

Fig. 3. Solid state part of the computed CaO-MgO phase diagram. Solid circles indicate experimentally determined solubility limits. Solid curves indicate the computed miscibility gaps with and without the effect of vibrational entropy. The Horizontal line indicates the experimental eutectic temperature and has no relation to the top of the miscibility gap.

for phase diagrams can be made without any prior need for experimental data on the system. In the next section, we apply a similar technique to a more complex oxide mixture.

4. The Gd_2O_3-ZrO_2 Phase Diagram

Zirconia (ZrO_2) mixed with oxides with lower-valent cations is a technologically important material. Its high oxygen diffusivity at elevated temperature makes it suitable as an electrolyte in sensor and fuel-cell applications. Even modest improvements to the diffusivity of oxygen are expected to lead to substantial economical benefits [14,15]. As in many oxides, the cations have very slow diffusion rates making it difficult to determine the equilibrium phase diagram of this system with experimental means.

Although pure ZrO_2 can exist in several crystal structures we will only deal here with the cubic fluorite structure which is stabilized at high temperature or with sufficient doping with lower valent cations. Two problems arise when modeling Gd_2O_3-ZrO_2 mixtures on the fluorite lattice. Gd_2O_3 not only introduces disorder on the cation sublattice but also on the oxygen sublattice through the introduction of charge compensating oxygen vacancies. Because the system exhibits binary disorder on two sublattices, its coarse-grained energy model needs to be expanded with the coupled-cluster basis functions of Eq. (6). This significantly increases the number of ECI as both intra-sublattice (cation-cation and anion-vacancy) and inter-sublattice (cation-vacancy) terms need to be calculated. In addition, as the ECI now describe exchange of species with different nominal charge the electrostatic interaction may increase the range at which they converge. Special techniques to deal with this convergence problem have been developed [16] and will be used in this work.

For this system the energy input was obtained from a simple empirical potential model in which ions electrostatically interact as point charges. The repulsive energy at short distances was parameterized with a Buckingham potential with parameters taken from [17] and [18]. With this model, the energies of 165 ordered arrangements of cations and anions were computed in order to fit a coupled cluster expansion with 41 ECI. The 165 ordered structures were derived by constructing all possible arrangements of the ions in small cells. Structures with very high energy where discarded as it can be shown that they do not influence the ECI [16]. The volume and all internal coordinates of the structures were relaxed. We did not relax the cell-*shape*. The large input needed in this case to parameterize the cluster expansion, prohibits the use of more accurate quantum mechanical energy techniques. Because of the relatively simple energy model used and the lack of cell-shape relaxation, the results should only be expected to reproduce the real system in a qualitative manner.

From the formation energy of the 165 structures, we found that the model predicts two stable compounds: the pyrochlore structure at composition $Zr_2Gd_2O_7$ and the bixbyite structure at composition Gd_2O_3. Both structures are observed experimentally. Internal relaxations were found to be essential to stabilize these structures. If only the electrostatic energy between ions on the sites of a rigid fluorite lattice is considered, neither the bixbyite nor the pyrochlore structure is stable. The latter is more than 3 eV above the lowest energy structure with the same composition.

The equilibrium phase diagram was computed by Monte Carlo simulation in a mixed canonical grand-canonical scheme [19] on a cell with 512 cation and 1024 anion sites. The predicted phase diagram is shown in Fig. 4. Although the temperature scale is strongly overestimated, the diagram clarifies several essential features of the system. The pyrochlore compound, in which both the anions and the cations are ordered at low temperature, transforms to a disordered fluorite structure through a first order transition. Based on some X-ray diffraction measure-

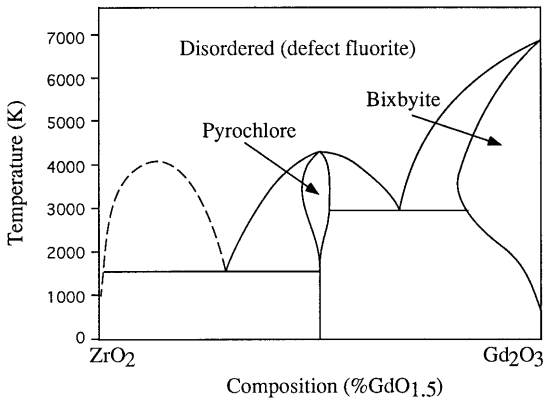

Fig. 4. Solid state part of the computed ZrO_2-Gd_2O_3 phase diagram. Transition temperatures are overestimated due to the approximations in the energy model.

ments on samples quenched from different temperatures it has been speculated [20] that both cation and anion sublatticies may undergo a separate order-disorder transition. Our results clearly do not support this claim and show a single order-disorder transition from the pyrochlore to the disordered fluorite phase. It is more likely that the experimental observations reflect a state in which the cations were short-range ordered. In our simulations we found that there is considerable short-range order in the fluorite phase above the order-disorder transition temperature. Figure 5 shows diffuse scattering along the [111] fluorite direction calculated from the Monte Carlo simulation. The temperature was just above the pyrochlore transition temperature. The sharp features in the scattering around the position where the superstructure peak for the pyrochlore phase would be located ($k = 0.5$) indicate relatively large domains of pyrochlore-like ordering in the disordered state.

At high Gd_2O_3 concentration, there is a large solubility of ZrO_2 in the low-temperature bixbyite. At lower concentration of Gd_2O_3 we also predict a region in which the solid solutions unmix (dashed line).

The phase diagram at very low and high concentrations of Gd_2O_3 is not the actual equilibrium phase diagram of this system. At low temperature and low concentration of Gd_2O_3, ZrO_2 is either tetragonal or monoclinic and not cubic as assumed here. At higher temperatures, the actual system forms phases that are not described by arrangements on the fluorite lattice.

The output of the calculations provides a much more detailed description of the system than can be represented in the phase diagram. Recently, the configurations, obtained from simulations, were used to explain the dependence of the oxygen-ion conductivity on the doping concentration in this material [19].

This example shows that even fairly complex systems can be treated with the procedure outlined in section 2. Currently, only the lack of a fast, more

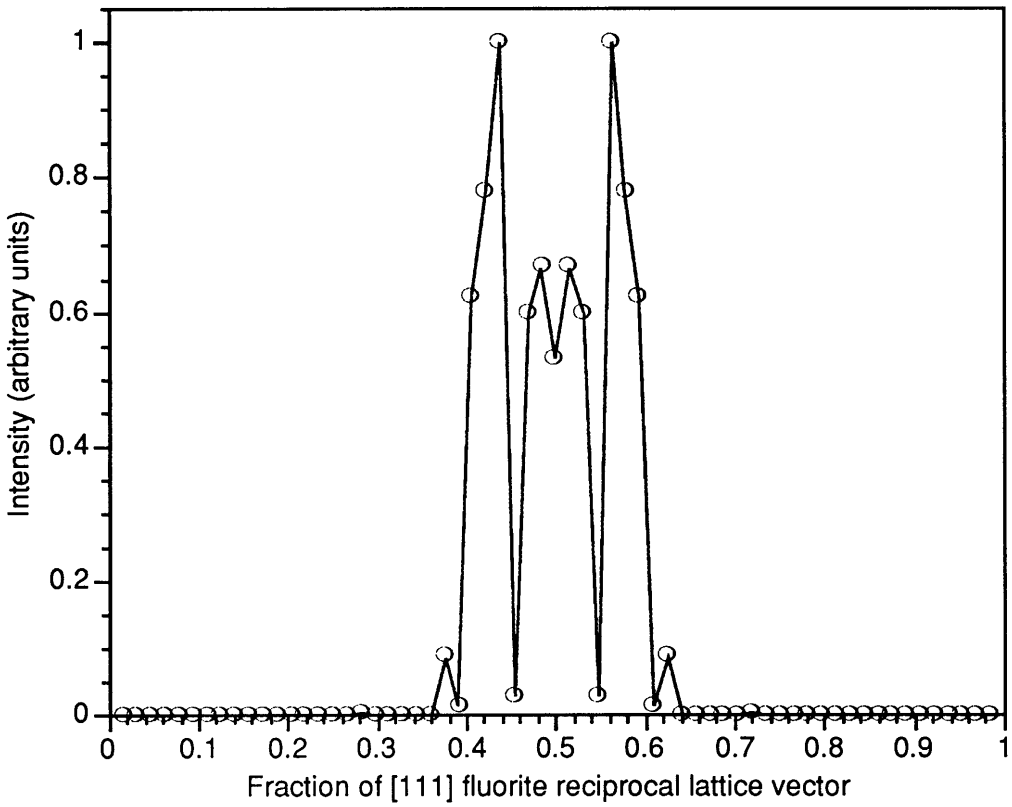

Fig. 5. Computed diffraction intensity along the [111] direction for the disordered fluorite phase. The ordered pyrochlore would have a superstructure peak at [0.5 0.5 0.5].

accurate energy description prohibits the first-principles calculation of these systems. Progress on a relatively fast and accurate energy method for oxides has recently been reported [11] and work to extend that approach to this system is currently under way in our group.

5. Sodium β″-alumina

Sodium β''-alumina is a fast-ion conductor used as a solid electrolyte for the sodium/sulphur battery. The most common β''-alumina is magnesium stabilized sodium β''-alumina with composition $Na_{1+x}Mg_xAl_{11-x}O_{17}$ where $x \approx 0.67$ [21,22]. In this section we determine the preferred Mg ordering and its effect on the Na ordering.

The Al^{3+} and Mg^{2+} ions reside in spinel blocks of the β''-alumina structure (Fig. 6). These spinel blocks are separated by relatively open low density 'conduction' planes containing sodium and oxygen ions. Ionic conductivity is localized in these planes. In

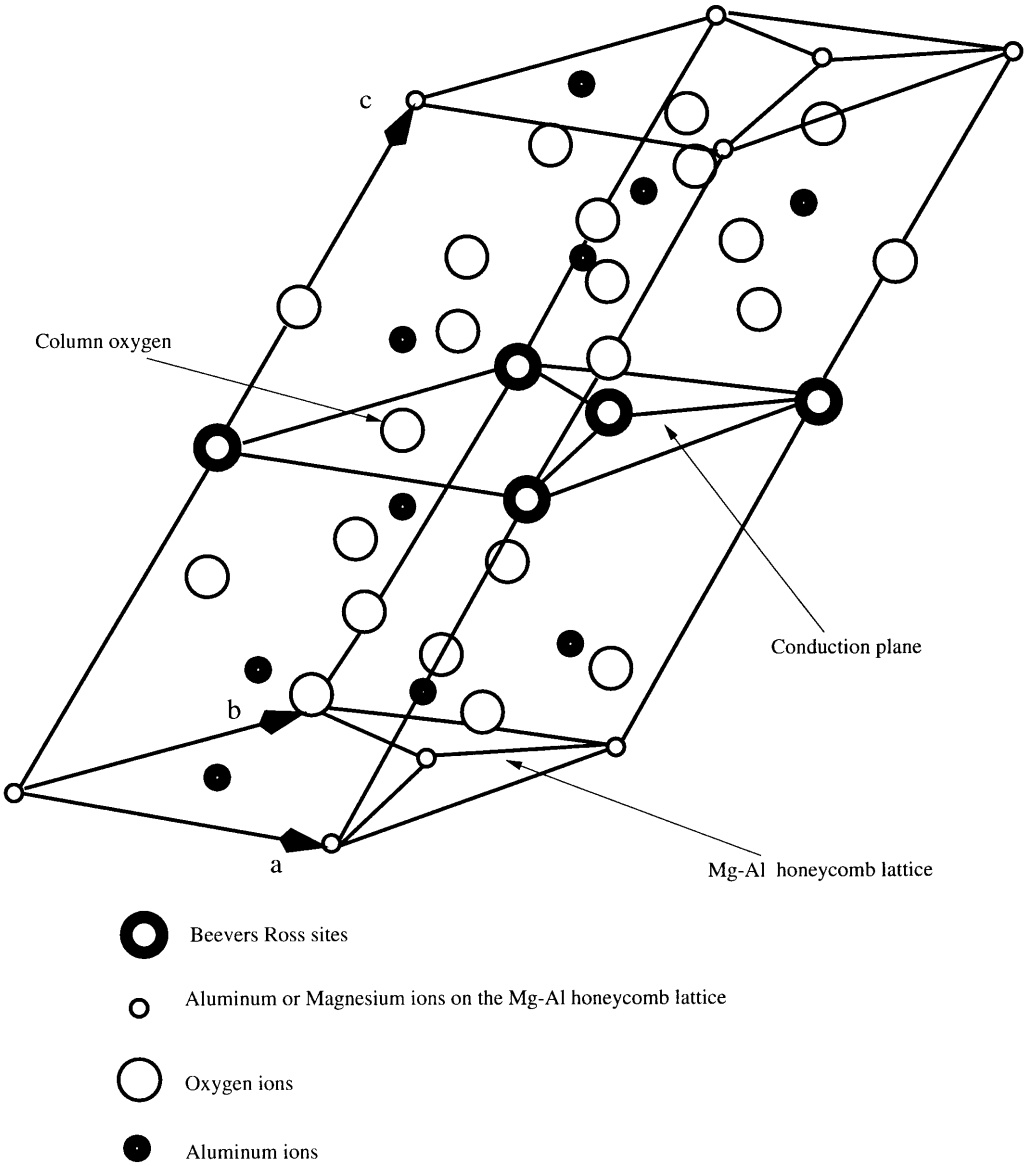

Fig. 6. Unit cell of sodium β''-alumina represented in the compact monoclinic unit cell. The sodium conduction planes are separated by blocks with the spinel structure.

the spinel blocks, the Al^{3+} reside in four crystallographically distinct interstitial sites. Computational [23] and experimental [21,22] evidence indicate that Mg^{2+} ions substitute in only one of these interstitial sites. The latter sites form a two-dimensional honeycomb lattice centered in the spinel blocks (see Fig. 6). In slowly cooled crystals the Na ions order below 200°C in $\sqrt{3}a \times \sqrt{3}a$ supercell [22]. At higher temperature the Na ions are disordered on sites that lie along a two-dimensional honeycomb lattice formed by the BR-sites (see Fig. 6).

In quenched crystals of β''-alumina the temperature-dependence of the ionic conductivity shows the usual Arrhenius behavior [24]. This behavior is strikingly different in slowly cooled samples where the activation energy changes over a narrow temperature interval centered around 200°C [22,24–26]. At high temperature ($T > 600$ K), the activation energy is 0.10 eV, while at low temperature ($T < 400$ K), the activation energy is 0.33 eV [22]. Both experimental evidence and molecular dynamics simulations seem to suggest that there is a close connection between the non-Arrhenius behavior and the formation of the sodium superstructure below 200°C [22,27–29]. It has been suggested that the increased activation energy at low temperatures results from the pinning of vacancies in the conduction plane as a result of the Na ordering [22,30]. Thus, the absence of a change in the activation energy in the quenched samples has been attributed to the suppression of the Na ordering in these samples as a result of the quench treatment [27]. In fact, neutron diffraction experiments have indicated that the sodium ordering in the quenched crystals is significantly lower than in the slowly cooled samples [27]. The high mobility of the Na ions makes it unlikely that a high temperature disordered Na configuration has been frozen in at low temperatures in the quenched samples. Instead, a more plausible explanation for the difference in Na

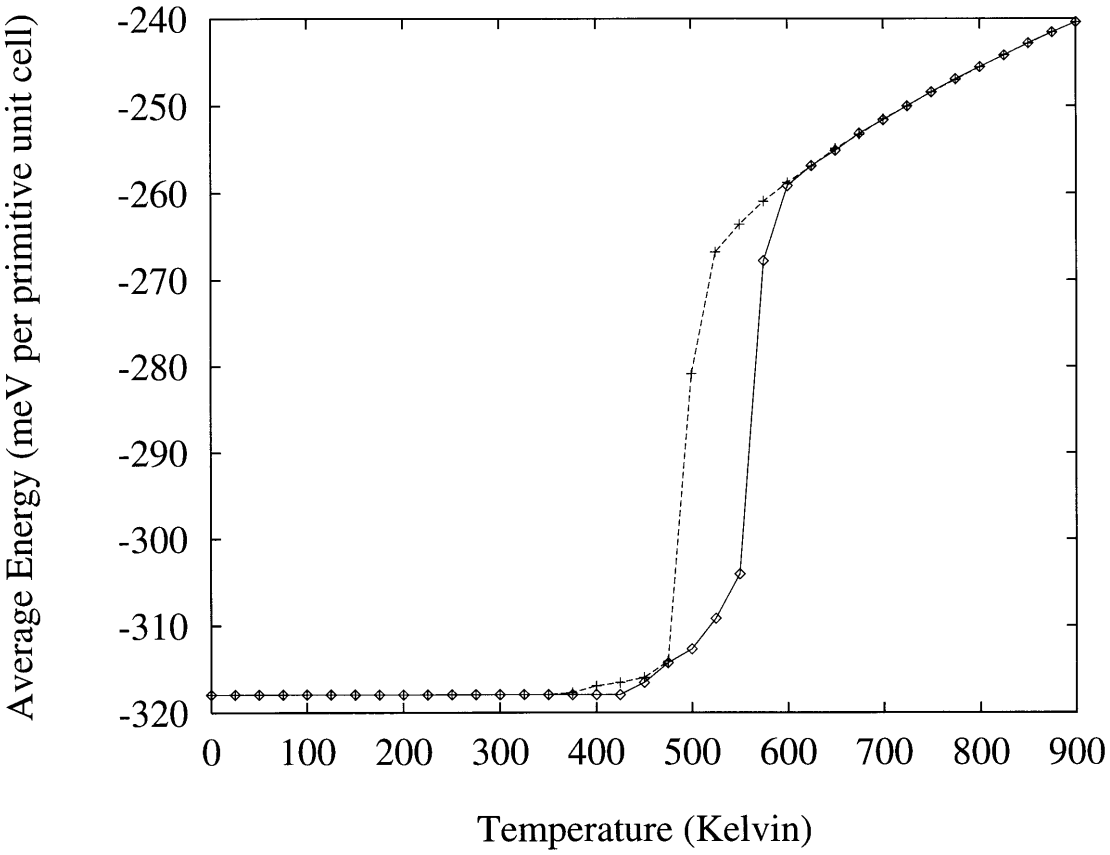

Fig. 7. Average energy in the Monte Carlo simulation as function of temperature in a heating (solid line) and cooling (broken line) simulation.

ordering between quenched and slowly cooled crystals, offered by Davies et al. [24] and Alden et al. [27], is that different thermal treatments results in variations in the Mg and Al ordering in the close packed spinel blocks, which in turn affects the degree of Na ordering. Lane-Rohrer [31] and Hafskjold [28] used Molecular Dynamics simulations on β''-alumina to investigate the influence of the Mg^{2+} configuration in the spinel blocks on sodium conductivity and found a substantial effect. The Mg^{2+} configurations in these simulations had to be picked arbitrarily as the kinetics of ordering in the spinel blocks is too slow to study with Molecular Dynamics simulation. Using the coupled sublattice technique we can actually predict the equilibrium ordering in both the spinel blocks and the conduction

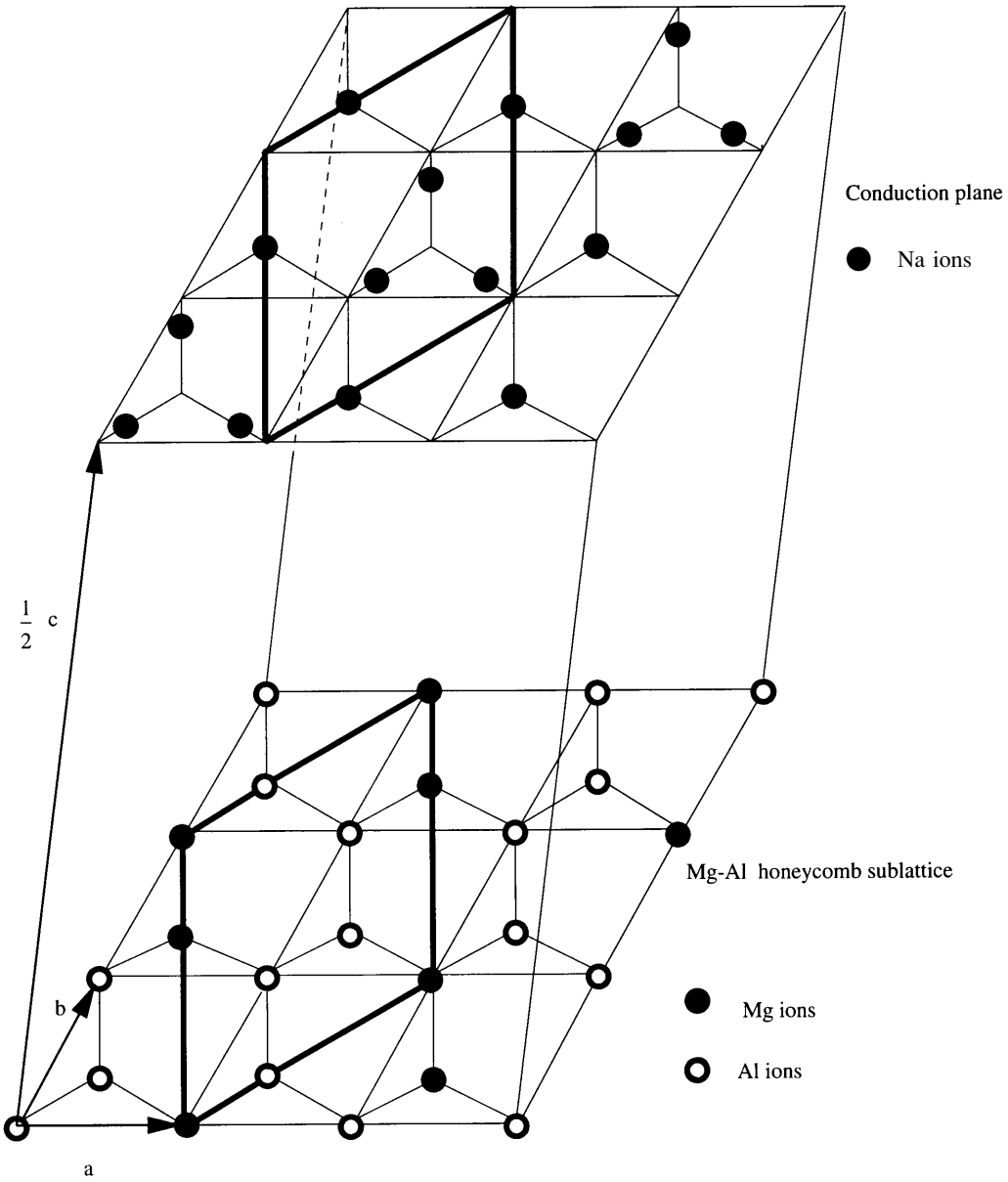

Fig. 8. Stable equilibrium ordering in the sodium conduction plane (top plane) and Mg-Al plane (bottom plane). Lattice vectors correspond to those of the primitive unit cell of β"- alumina (see Fig. 6).

planes. We can also investigate the effect of the shift in disorder temperature for the sodium ordering caused by various degrees of quenched Mg^{2+}-Al^{3+} disorder.

The cluster expansion for this material was parameterized by computing the energy of 129 different configurations of Na^{+} in the conduction planes and Mg^{2+} and Al^{3+} in the spinel blocks with an empirical pair potential model. The parameters of the model were the same as those used in a previous Molecular Dynamics simulation [28]. The behavior of the system at non-zero temperature was studied by Monte Carlo simulation on a cell containing 864 primitive unit cells and at fixed composition. Figure 7 shows the energy of the system as a function of temperature for heating (solid line) and cooling (dashed line) simulations. The discontinuity in the energy around 500 K indicates an order-disorder transition in the system. The hysteresis reflects the first-order character of the transition. The stable Mg ordering obtained below 500 K is shown in Fig. 8 (lower plane). This is the first time that the equilibrium Mg configuration has been reported. The Na ordering observed in the simulation is shown in the top plane of Fig. 8 and is the same as the one observed by Boilot et al. [22]. Remarkably, the stable ordering in the Mg-Al plane and in the Na-conduction plane have the same unit cell size and shape.

Similarly to the pyrochlore-to-fluorite transition in $Zr_2Gd_2O_7$, the strong coupling between the two sublattices in sodium β''alumina results in a single order-disorder transition at which both the Na and the Mg ions disorder simultaneously.

In reality, it is unlikely that the Mg-Al ordering will fully equilibrate due to the slow diffusion in the spinel blocks. It is therefore of interest to simulate the effect of quenched-in disorder on the Mg sublattice: This was done by creating a high temperature Mg

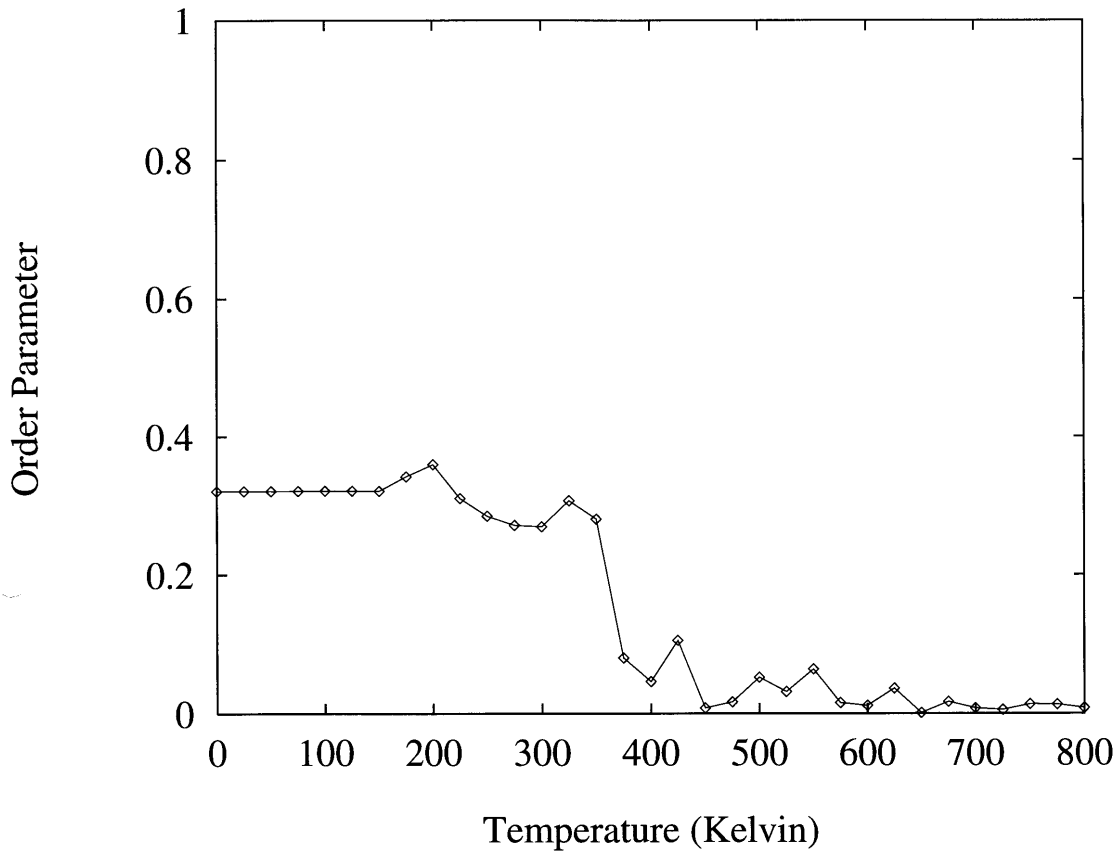

Fig. 9. Order parameter for the sodium ions as a function of temperature for a material with quenched-in Mg disorder. Below 350 K the system settles into patches of ordered and disordered sodium regions resulting in an order parameter between 0 and 1 in the honeycomb sublattice.

configuration (obtained by annealing the system at 1725 K) and freezing it in the subsequent cooling runs. Hence, after the high-temperature anneal, only the sodium configuration was sampled in the Monte Carlo simulations. Remarkably, the Na ions still order into the $\sqrt{3}a \times \sqrt{3}a$ superstructure, however, the ordering is imperfect and occurs at a lower temperature. Figure 9 shows the order parameters in the Na plane. The order parameter is defined so that it has the value 1 for a perfectly ordered state and zero for a completely random state. At 500 K, the equilibrium transition temperature, the Na ions remain fully disordered. Below 300 K the Na ions clearly order. Although the order parameters abruptly changes at 300 K, no discontinuity was found for the average energy near 300 K. This is to be expected as the fluctuating field arising from the disordered Mg ions smears the order-disorder transition in the Na-conduction plane.

The results not only clarify the equilibrium Mg configuration in the system but also indicates how different thermal treatments may influence the Na conductivity. In equilibrium, Na and Mg ions order simultaneously below $\sim$500 K. When rapid cooling prevents Mg ordering, the Na ordering is depressed to lower temperatures. This effect is expected to increase the Na conductivity since the activation energy for Na conduction is lower in the disordered state than in the ordered state. From our results one can speculate that long-term aging may reduce the Na conductivity by allowing the Mg ions to order, thereby increasing the level of Na ordering. Given the empirical potential model used as input for this model, the quantitative agreement between the calculated temperatures and experimental data may in this case be somewhat fortuitous.

6. Conclusion

The information contained in equilibrium phase diagrams is essential to gain an understanding in the relation between structure, thermal processing and composition for a material. Phenomena on time scales spanning 10 orders of magnitude contribute to the equilibrium free energy of a system preventing the use of direct simulation techniques such as Molecular Dynamics. One therefore has to rely on procedures to systematically integrate over the faster degrees of freedom to obtain a Hamiltonian for the slowest degrees of freedom. In most cases, the slowest time-scale is set by the substitutional disorder so that the final Hamiltonian will have the form of a lattice model Hamiltonian. The cluster expansion technique provides an excellent way to obtain an explicit expression for this Hamiltonian.

The second problem with phase diagram prediction is the required accuracy. The model for the energy of the system needs to be accurate on the scale of kT. At 1000°C, kT is $\approx$100 meV. Only quantum mechanical models can be expected to give mixing energies to such accuracy. It is therefore not unexpected that simpler energy models woefully overestimate the temperature scales. In all cases we attempted so far, empirical potential models, commonly used in oxides, did reproduce the qualitative features of the phase diagram.

Clearly, most of the building blocks for the first-principles calculations of phase diagrams are in place. If the results in the CaO-MgO system are indicative of the accuracy that can be obtained with our approach, we can expect to predict phase diagrams that are topologically correct and have transition temperatures accurate within 10 to 20%. Currently, the application of first-principles calculations to more complex systems is limited by the large amount of calculations required to parameterize the cluster expansion.

Given the wealth of information contained in the output of atomic-level calculations such as the ones presented here, it seems inevitable that they will lead to a better characterization of oxide systems and contribute to a better understanding of the behavior of these materials.

Acknowledgments

This work was supported in part by the MRSEC Program of the National Science Foundation under Award Number DMR-9400334, by the National Science Foundation under contract DMR-9501856 and by a Petroleum Research Fund Grant PRF-29133-AC5.

References

1. G. Ceder, *Computational Materials Science*, **1**, 144–150 (1993).
2. J.M. Sanchez, F. Ducastelle, and D. Gratias, *Physica*, **128A**, 334–350 (1984).
3. G. Ceder, G.D. Garbulsky, K. Fukuda, and D. Avis, *Phys. Rev. B*, **49**, 1–7 (1997).

4. R. McCormack, D. de Fontaine, C. Wolverton, and G. Ceder, *Phys. Rev. B*, **51**, 15808–15822 (1995).
5. P.D. Tepesch, G.D. Garbulsky, and G. Ceder, *Phys. Rev. Lett.*, **74**, 2272–2275 (1995).
6. L. Anthony, J.K. Okamoto, and B. Fultz, *Phys. Rev. Lett.*, **70**, 1128–1130 (1993).
7. G.D. Garbulsky and G. Ceder, *Phys. Rev. B*, **53**, 8993–9001 (1996).
8. Y. Yin and B.B. Argent, *J. Phase Equilibria*, **14**, 588–600 (1993).
9. P.D. Tepesch, A.F. Kohan, G.D. Garbulsky, G. Ceder, C. Coley, H.T. Stokes, L.L. Boyer, M.J. Mehl, B. Burton, K. Cho, and J.Joannopoulos, *J. Am. Ceram. Soc.*, **79**, 2033–2040 (1996).
10. G.D. Garbulsky and G. Ceder, *Phys. Rev. B*, **49**, 6327–6330 (1994).
11. A.F. Kohan and G. Ceder, *Phys. Rev. B*, **54**, 805–811 (1996).
12. M.C. Payne, M.P. Teter, D.C. Allan, T.A. Arias, and J.D. Joannopoulos, *Rev. Mod. Phys.*, **64**, 1045 (1992).
13. L.L. Boyer and M.J. Mehl, *Ferroelectrics*, **150**, 13–24 (1993).
14. K. Krist and J.D. Wright, in *Solid Oxide Fuel Cells*, S.C. Singhal and H. Iwaharas, Eds., vol. 93–4, pp. 782–791.
15. B.C.H. Steele, in *Electronic Ceramics*, B.C.H. Steele, ed. (Elsevier, London, 1991) pp. 203–226.
16. G. Ceder, G.D. Garbulsky, and P.D. Tepesch, *Phys. Rev. B*, **51**, 11257–11261 (1995).
17. M.P. van Dijk and A.J. Burggraaf, *Solid State Ionics*, **17**, 159–167 (1985).
18. A. Dwived and A.N. Cormack, *Journal of Solid State Chemistry*, **79**, 218–231 (1989).
19. P. Tepesch, PhD thesis, Massachusetts Institute of Technology (1996).
20. T. Moriga, S. Emura, A. Yoshiasa, S. Kikkawa, F. Kanamaru, and K. Koto, *Solid State Ionics*, **40**, 357–361 (1990).
21. W.L. Roth, F. Reidinger, and S. La Placa, in *Superionic Conductors*, G. Mahan and W.L. Roths, Eds., pp. 223 (1976).
22. J.P. Boilot, G. Collin, P. Colomban, and R. Comes, *Phys. Rev. B*, **22**, 5912 (1980).
23. L. Xie and A.N. Cormack, *Materials Letters*, **9**, 474–479 (1990).
24. P.K. Davies, F. Garzon, T. Feist, and C.M. Katzan, *Solid State Ionics*, **18/19**, 1120 (1986).
25. J.L. Briant and G.C. Farrington, *J. Solid State Chem.*, **33**, 385 (1980).
26. H. Engstrom, J.B. Bates, W.E. Brundage, and J.C. Wang, *Solid State Ionics*, **2**, 265 (1981).
27. M. Alden, J.O. Thomas, and P. Davies, *Solid State Ionics*, **18/19**, 694 (1986).
28. B. Hafskjold and X. Li, *Condens. Matter*, **7**, 2949 (1995).
29. W. Smit and M.J. Gillan, *J. Phys.: Condens. Matter*, **4**, 3215 (1991).
30. J.C. Wang, J.B. Bates, N.J. Dudney, and H. Engstrom, *Solid State Ionics*, **5**, 35 (1981).
31. C. Lane-Rohrer and G.C. Farrington, *Chem. Mater.*, **4**, 55 (1991).